INORGANIC CHEMISTRY FRONTIERS

RESEARCH ARTICLE

View Article Online
View Journal | View Issue

Cite this: *Inorg. Chem. Front.*, 2023, **10**, 4711

Searching for silicate nonlinear optical materials by combining calculation and experiment†

Jingjing Zhang, Ruqing Wei, Daqing Yang, Ying Wang and Bingbing Zhang *

Received 26th May 2023,
Accepted 8th July 2023

DOI: 10.1039/d3qi00979c

rsc.li/frontiers-inorganic

Nonlinear optical (NLO) materials have been applied in many high technology fields. In this work, the first-principles high-throughput screening pipeline (FHSP) has been used for searching NLO materials from the silicate system. 253 silicates collected in the Inorganic Crystal Structural Database (ICSD) have been successfully calculated. Among them, 8 crystals were screened out after two-step evaluation. Finally, 3 compounds were selected for synthesis after comprehensive investigation. The SHG intensities tested using the Kurtz–Perry method of $KNbSi_2O_7$, $PbZnSiO_4$, and Na_2TiSiO_5 are 6.7, 2.9, and 2.8 times that of KDP, respectively. Their UV absorption edges are 243 nm, 276 nm, and 280 nm, respectively. This work provides a full view of silicates as NLO materials and obtains excellent candidates for the next step of development.

Introduction

Nonlinear optical (NLO) crystals are key materials in laser systems owing to their functions of frequency conversion, generation of entangled photon pairs, attosecond pulse generation, *etc.*[1–5] Frequency conversion through NLO materials is a convenient and efficient approach to generate laser beams in a wider range.[6–8] β-BaB_2O_4 (BBO),[9] LiB_3O_5 (LBO),[10] $AgGaSe_2$ (AGSe),[11] $AgGaS_2$ (AGS),[12] and $ZnGeP_2$ (ZGP)[13] are commercialized materials that are widely used in the ultraviolet (UV) and mid-far-infrared (M-F-IR) wavelength range.[14] With the development of laser technology, NLO crystals with optimal performance are urgently required.

Silicates have wide transmission ranges from ultraviolet to mid-IR such as those of $Bi_{12}SiO_{20}$ (0.37–6.0 μm),[15,16] $Ba_2TiOSi_2O_7$ (0.3–5.0 μm),[17] Y_2SiO_5 (0.2–5.0 μm), Gd_2SiO_5 (0.2–5.0 μm), and Lu_2SiO_5 (0.2–5.0 μm).[18] In addition, the silicate system has potential to generate large SHG coefficients, such as those of $Li_2K_4[(TiO)Si_4O_{12}]$ (4.5 × KDP) and $Li_2Rb_4[(TiO)Si_4O_{12}]$ (4.5 × KDP),[19] $Ba_2TiOSi_2O_7$ (5.5 × KDP),[17] $PbSrSiO_4$ (5.8 × KDP),[20] $Sr_2TiSi_2O_8$ (8.0 × KDP),[21] and $Cs_2B_4SiO_9$ (4.6 × KDP).[22] Besides, silicates usually exhibit large band gaps and correspondingly high laser-induced damage thresholds (LDTs), as well as stability in open air.

In this work, non-centrosymmetric silicate crystals collected in the Inorganic Crystal Structural Database (ICSD) are comprehensively investigated using the first-principles high-throughput screening pipeline for NLO materials (FHSP-NLO) and experimental confirmation.[23] Finally, three silicates, $KNbSi_2O_7$, $PbZnSiO_4$, and Na_2TiSiO_5, meeting strict multiple criteria are screened out and synthesized using a high-temperature solid-state method. They possess excellent properties, including large SHG coefficients, suitable birefringence, and short cut-off edges. In addition, statistical analysis based on the different classification of cations shows that d^0-transition metal (TM) and lone pair (LP) cations play a vital role in birefringence and SHG response.

Methods

Synthesis

$KNbSi_2O_7$, $PbZnSiO_4$, and Na_2TiSiO_5 were synthesized by the conventional solid-state method. The initial reagents including SiO_2 (Aladdin, 99%), K_2CO_3 (Aladdin, 99.5%), Nb_2O_5 (Aladdin, 99.9%), PbO (Aladdin, 99.9%), ZnO (Aladdin, 99%), NaOH (Aladdin, 95%) and TiO_2 (Aladdin, 99%) were used without further purification. Stoichiometric amounts of reactants were mixed thoroughly and heated in the corundum crucibles. The reactants, reaction time, and temperature for each compound are listed below.

$KNbSi_2O_7$. $KNbSi_2O_7$ was synthesized using K_2CO_3 (0.086 g), Nb_2O_5 (0.166 g), and SiO_2 (0.150 g). After weighing the raw materials, they were ground evenly, and the mixtures were transferred into an alumina crucible. The mixtures were

College of Chemistry and Materials Science, Key Laboratory of Medicinal Chemistry and Molecular Diagnosis of the Ministry of Education, Key Laboratory of Analytical Science and Technology of Hebei Province, Hebei University, Baoding 071002, China. E-mail: zhangbb@hbu.edu.cn

†Electronic supplementary information (ESI) available: Calculated band structure and partial density of states (PDOS) of $PbZnSiO_4$ and Na_2TiSiO_5. The chemical formula, ICSD collection-code, space group, band gap (E_g), birefringence (Δn), second-order susceptibility ($\chi^{(2)}$), and maximum $\chi^{(2)}$ tensor ($|\chi^{(2)}|_{max}$) of all 253 silicates. Database is accessed by visiting **https://nlo.hbu.cn**. See DOI: **https://doi.org/10.1039/d3qi00979c**

heated from room temperature to 1170 °C in 5 h, held at that temperature for 24 h, cooled to 1100 °C in 70 h, then cooled to 1000 °C in 72 h, and finally cooled to room temperature in 24 h.

$PbZnSiO_4$. $PbZnSiO_4$ was obtained using PbO (1.114 g), ZnO (0.406 g), and SiO_2 (0.300 g). The mixtures were heated from room temperature to 750 °C in 3 h, held at that temperature for 72 h, and cooled to room temperature in 3 h. The mixtures were then removed and thoroughly ground. The same method was used for refiring twice to improve the purity of the material.

Na_2TiSiO_5. Na_2TiSiO_5 was synthesized using NaOH (0.200 g), TiO_2 (0.200 g), and SiO_2 (0.150 g) as raw materials. The mixtures were heated from room temperature to 850 °C in 6 hours and kept at this temperature for 10 hours, then finally cooled to room temperature in 3 h.

Powder XRD

$KNbSi_2O_7$, $PbZnSiO_4$, and Na_2TiSiO_5 were tested using a Bruker-D8 X-ray diffractometer. The experimental XRD spectra of the title compounds were measured using X-rays with Cu Kα radiation (λ = 1.541 Å) at room temperature, and then compared with the theoretical XRD pattern.

Infrared spectroscopy

The IR spectra of $KNbSi_2O_7$, $PbZnSiO_4$, and Na_2TiSiO_5 were recorded on an IR Affinity-1 Fourier transform infrared spectrometer (Nicolet iS10, America) in the range of 400–3000 cm^{-1}. The silicates were ground and mixed with KBr.

UV-vis-NIR diffuse-reflectance spectra

The UV-vis-NIR diffuse reflectance spectra of $KNbSi_2O_7$, $PbZnSiO_4$, and Na_2TiSiO_5 were measured at room temperature with a SolidSpec-3700DUV spectrophotometer. The wavelengths of the spectra were in the range 190–1100 nm.

SHG measurement

Through the Kurtz-Perry method,[24] the powder SHG (PSHG) responses of $KNbSi_2O_7$, $PbZnSiO_4$, and Na_2TiSiO_5 were investigated using a Q-switch laser at 1064 nm. Silicates and KDP were ground and sieved into different particle size ranges: 20–38, 38–55, 55–88, 88–125, 125–160, 160–200, and 200–250 μm.

Computational method

Theoretical calculations were performed using the CASTEP package based on density functional theory (DFT).[25] The CASTEP package has been used to perform self-consistent field (SCF) and optical calculations with normal conserved pseudopotentials (NCPs). The exchange correlation energy is described by the Perdew–Burke–Ernzerhof (PBE) functional within the generalized gradient approximation (GGA).[26,27] The energy cutoff of the plane-wave base was set to 750 eV. The SCF calculations were performed with a convergence criterion of 1×10^{-6} eV per atom on total energy. Numerical integration of the Brillouin zone was performed using the Monkhorst–Pack scheme with k-point separation set as 0.07 $Å^{-1}$ in the Brillouin zone for SCF and 0.04 $Å^{-1}$ for optics calculation. The empty band was set to 3 times the valence band in the optical calculation to ensure the convergence of the refractive index and SHG coefficients.

Results and discussion

First, 279 noncentrosymmetric (NCS) structures containing Si and O elements were obtained from the Inorganic Crystal Structural Database (ICSD). Then, the band gap, birefringence, and second-order susceptibility $\chi^{(2)}$ of these silicates were calculated using FHSP-NLO. Finally, 253 structures were calculated successfully. The chemical formula, ICSD collection-code, space group, band gap (E_g), birefringence (Δn), second-order susceptibility ($\chi^{(2)}$), and the maximum $\chi^{(2)}$ tensor of all 253 structures are listed in the ESI.† As shown in Fig. 1, the maximum $\chi^{(2)}$ tensors of these silicate crystals are plotted against their band gaps E_g-GGA. One can easily find that the maximum $\chi^{(2)}$ obviously decreases with the increase in the band gap, which is consistent with the theory.

As we mentioned above, silicates have a wide transmission window from UV to mid-IR and accordingly they can be used as NLO materials working in a wide wavelength range. In order to screen the materials that meet the conditions from UV to mid-IR, we adopted a new screening method. Firstly, we screened out the structures that meet the criteria for UV NLO crystals, *i.e.* E_g > 6.0 eV and $\chi^{(2)}$ > 0.78 pm V^{-1}. Secondly, the structures that meet the criteria for IR NLO crystals (E_g > 2.5 eV and $\chi^{(2)}$ > 7.8 pm V^{-1}) were screened out. Thirdly, we joined the two points (marked as G (2.5, 7.8) and H (6, 0.78)) with a straight line. Then, the materials located to the top-right of this line were screened out. Finally, 17 structures (located in the green shading of Fig. 1) with excellent properties were selected.

The calculated properties of the selected 17 structures are listed in Table 1. There are 14 materials because some struc-

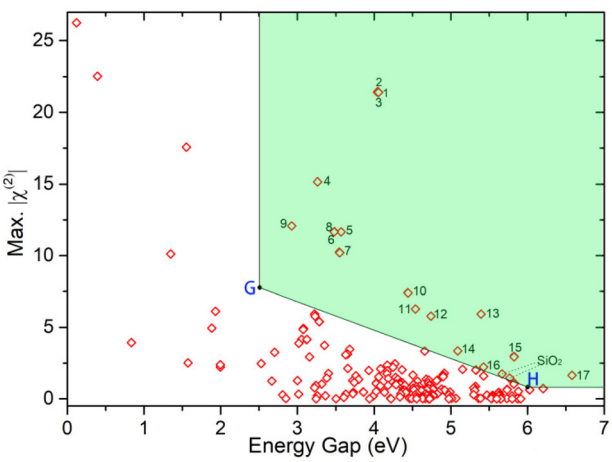

Fig. 1 The statistical chart of calculated results for 253 silicates.

Table 1 Chemical formulas, ICSD collection numbers, space groups (SG), calculated band gaps both using GGA and HSE06 (E_g-GGA and E_g-HSE, units: eV), birefringences calculated using the SOS and DFPT method (Δn-SOS and Δn-DFPT) at 1064 nm, and SHG coefficients ($\chi^{(2)}$) of 17 selected materials. The scissor operators that are set as the difference between E_g-GGA and E_g-HSE are used in the calculation of $\chi^{(2)}$

No.	Formula	ICSD	SG	E_g-GGA (eV)	E_g-HSE (eV)	Δn-SOS	Δn-DFPT	$\chi^{(2)}$ (+scissor) (pm V^{-1})
1	$Ba_2TiSi_2O_8$	201 844	*P4bm*	4.05	5.82	0.060	0.034	$\chi_{113} = \chi_{223} = -3.064$, $\chi_{333} = 10.654$
2	$Ba_2TiSi_2O_8$	201 845	*P4bm*	4.05	5.83	0.061	0.035	$\chi_{113} = \chi_{223} = -3.039$, $\chi_{333} = 10.631$
3	$Ba_2TiSi_2O_8$	4451	*P4bm*	4.06	5.78	0.060	0.033	$\chi_{113} = \chi_{223} = 3.077$, $\chi_{333} = -10.835$
4	$PbZn(SiO_4)$	26 840	$Pna2_1$	3.26	4.21	0.033	0.045	$\chi_{113} = -1.811$, $\chi_{223} = -1.134$, $\chi_{333} = 8.959$
5	$Pb_4Zn_2[(SO_4)(SiO_4)(Si_2O_7)]$	100 296	$P2_1$	3.57	4.69	0.011	0.009	$\chi_{112} = 0.513$, $\chi_{123} = 1.074$ $\chi_{222} = -7.164$, $\chi_{233} = 0.766$
6	Na_2TiSiO_5	259 048	$Pmc2_1$	3.48	5.30	0.026	0.046	$\chi_{113} = -1.787$, $\chi_{223} = -0.194$, $\chi_{333} = 5.454$
7	$Ca_2(SiO_4)$	182 053	$P6_3mc$	3.55	4.07	0.078	0.057	$\chi_{113} = \chi_{223} = -1.017$, $\chi_{333} = -7.814$
8	Na_2TiSiO_5	82 153	$Pmc2_1$	3.48	5.24	0.026	0.049	$\chi_{113} = -1.872$, $\chi_{223} = -0.178$, $\chi_{333} = 5.582$
9	$KNbSi_2O_7$	72 111	*P4bm*	2.93	5.32	0.125	0.071	$\chi_{113} = \chi_{223} = 2.971$, $\chi_{333} = -0.81$
10	$Ba(Li_2SiO_4)$	260 259	$P6_3mc$	4.44	5.72	0	0.001	$\chi_{113} = \chi_{223} = 0.085$, $\chi_{333} = -4.369$
11	$CaZr(Si_2O_7)$	203 131	*C2*	4.5	6.59	0.062	0.052	$\chi_{112} = -0.799$, $\chi_{123} = -1.858$ $\chi_{222} = -1.075$, $\chi_{233} = 1.562$
12	$BaBe(SiO_4)$	86 792	*Cm*	4.74	5.66	0.020	0.019	$\chi_{111} = -0.027$, $\chi_{113} = -2.262$, $\chi_{122} = 1.720$ $\chi_{133} = -2.666$, $\chi_{223} = -0.980$, $\chi_{333} = 3.162$
13	$BaY_6(Si_3B_6O_{24})F_2$	30 674	*P3*	5.40	6.73	0.033	0.045	$\chi_{111} = -\chi_{122} = -0.494$, $\chi_{113} = \chi_{223} = 2.517$ $\chi_{333} = -3.105$
14	$Ba_2Y_3(SiO_4)_2F_5$	290 289	*Pba2*	5.09	6.58	0.035	0.046	$\chi_{113} = -0.371$, $\chi_{223} = 0.401$, $\chi_{333} = -2.173$
15	$BaBe_2(Si_2O_7)$	263 133	$Pmn2_1$	5.83	7.58	0.017	0.006	$\chi_{113} = 0.384$, $\chi_{223} = 0.643$, $\chi_{333} = -1.620$
16	$CsSiB_3O_7$	255 774	$Pna2_1$	5.43	7.27	0.044	0.056	$\chi_{113} = -0.400$, $\chi_{223} = -0.962$, $\chi_{333} = 1.150$
17	$LiB(SiO_4)$	67 536	$I\bar{4}$	6.58	8.51	0.004	0.008	$\chi_{113} = -0.158$, $\chi_{123} = 0.705$, $\chi_{223} = 0.158$

tures are duplicated. It is well known that the PBE functional tends to underestimate the band gap. To obtain accurate predictions of the band gap, a HSE (hybrid screened exchange) functional was used to perform the band structure calculation.[28–30] Both the values, E_g-GGA and E_g-HSE, are listed in Table 1. Based on our previous calculations, it is found that the sum-over-states method cannot precisely predict the birefringence of materials that contain Ti or Nb element, such as $Ba_2TiGe_2O_8$.[31] To improve the accuracy of the birefringence calculation, the density-functional perturbation theory (DFPT) method was adopted for the selected structures. Then we screened the materials with birefringence calculated using the DFPT method greater than 0.04. Subsequently, 8 materials were selected from the above 14 materials, namely $PbZn(SiO_4)$,[32] Na_2TiSiO_5,[33] $Ca_2(SiO_4)$,[34] $KNbSi_2O_7$,[35] $CaZr(Si_2O_7)$,[36] $BaY_6(Si_3B_6O_{24})F_2$,[37] $Ba_2Y_3(SiO_4)_2F_5$,[38] and $CsSiB_3O_7$.[39] After investigation and experimental verification, we chose three materials for further synthesis and characterization, *i.e.* $KNbSi_2O_7$, $PbZnSiO_4$, and Na_2TiSiO_5. For the other materials, $Ca_2(SiO_4)$ shows a virtual vibration frequency that demonstrates the dynamic instability of its structure. Indeed, a centrosymmetric structure that is more reasonable than this NCS structure had been reported.[40] Actually, when we synthesized this material the obtained phase was a centrosymmetric structure. The synthesis temperature of $CaZr(Si_2O_7)$ is too high, and our laboratory conditions cannot meet the requirements. $BaY_6(Si_3B_6O_{24})F_2$ and $Ba_2Y_3(SiO_4)_2F_5$ are multiphase structures, and the pure phase products are difficult to obtain. The NLO properties of $CsSiB_3O_7$ have been reported by Sun and Lin *et al.*,[39] and its SHG effect is 0.8 times that of KDP.

The powder XRD spectra of $KNbSi_2O_7$, $PbZnSiO_4$, and Na_2TiSiO_5 match well with the simulated ones derived from the CIF data (see Fig. 2(a)–(c)). The Rietveld refinement of PXRD data of pure polycrystalline samples was performed (Fig. S1–S3†). The details of the Rietveld refinement of PXRD are provided in Table S1.† It verified the phase purity of the title compounds. In addition, the existence of the fundamental building blocks (FBBs) was confirmed using the experimental IR spectra.[41] The IR spectra of $KNbSi_2O_7$, $PbZnSiO_4$, and Na_2TiSiO_5 samples in the wavenumber range 400–3000 cm^{-1} are shown in Fig. 2(d)–(f). According to calculated IR spectrum and the experimental results of IR spectroscopy, the IR absorption band near 900 cm^{-1} belongs to the stretching vibration of SiO_4 tetrahedra. The IR absorption band from 600 to 400 cm^{-1} belongs to the bending vibration of SiO_4 tetrahedra.[42] In particular, in the compound $KNbSi_2O_7$, the IR spectral characteristic peak at 1234 cm^{-1} belongs to the Si–O–Si stretching vibration in the Si_2O_7 dimer. The peak at 706 cm^{-1} is due to the Nb–O stretching modes of NbO_6 octahedra. The above infrared results can confirm the existence of fundamental building blocks (FBBs) in the title compounds.

The crystal structure of $KNbSi_2O_7$ belongs to NCS polar space group *P4bm* with $a = b = 8.7404(8)$ Å, $c = 8.136(1)$ Å, $\alpha = \beta = \gamma = 90°$, $Z = 2$. In its structure, NbO_6 octahedrons are connected to each other by sharing *para*-position O atoms to form chains. The chains are further connected by a Si_2O_7 dimer to form a three-dimensional (3D) skeleton with channels where K atoms are located (see Fig. 3(a)). The UV-vis-NIR diffuse reflectance spectra of $KNbSi_2O_7$, $PbZnSiO_4$, and Na_2TiSiO_5 are shown in Fig. 4(a)–(c). The spectra indicate that $KNbSi_2O_7$ has a short UV cutoff edge of 243 nm, and the absorption edge of $KNbSi_2O_7$ is 4.31 eV, which is larger than those of $Li_2K_4[(TiO)Si_4O_{12}]$ and $Li_2Rb_4[(TiO)Si_4O_{12}]$.[19] $KNbSi_2O_7$ exhibits a strong SHG intensity of 6.7 times that of KDP under 1064 nm fundamental wave laser radiation (Fig. 4(d)). It is larger than those

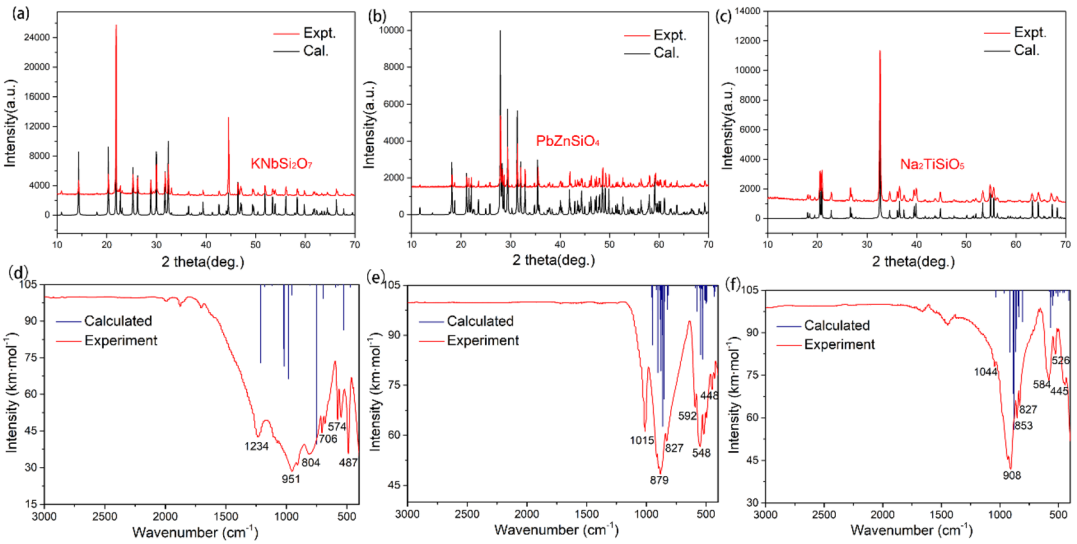

Fig. 2 Powder XRD of (a) $KNbSi_2O_7$, (b) $PbZnSiO_4$, and (c) Na_2TiSiO_5. Infrared spectroscopy of (d) $KNbSi_2O_7$, (e) $PbZnSiO_4$, and (f) Na_2TiSiO_5.

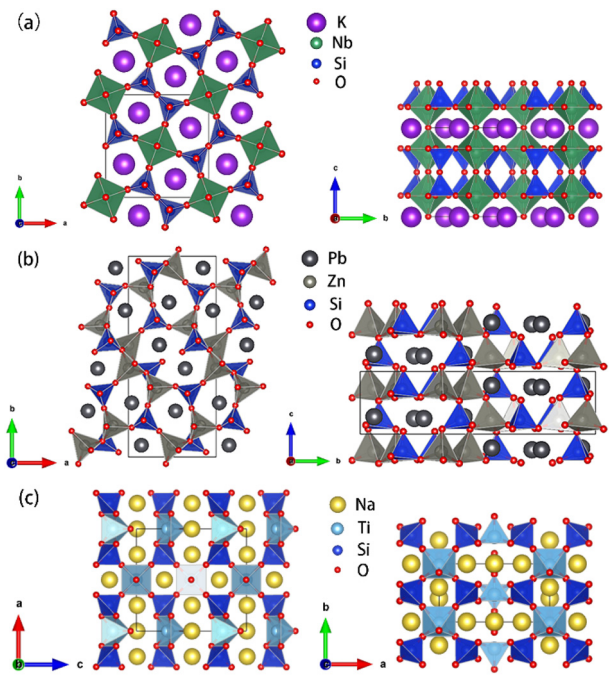

Fig. 3 (a) Crystal structures of $KNbSi_2O_7$. (b) Crystal structures of $PbZnSiO_4$. (c) Crystal structures of Na_2TiSiO_5.

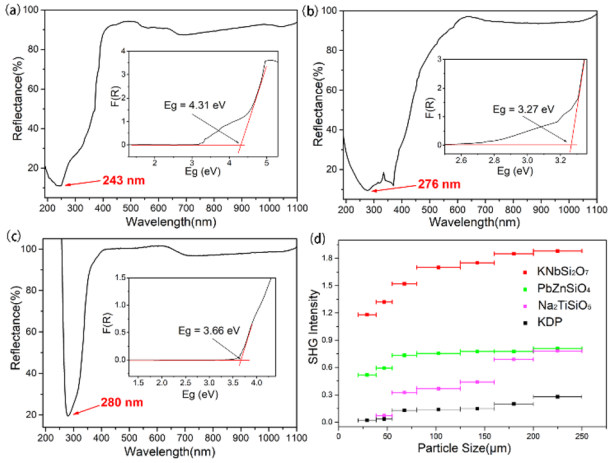

Fig. 4 UV–vis–NIR diffuse reflectance spectra of (a) $KNbSi_2O_7$, (b) $PbZnSiO_4$, and (c) Na_2TiSiO_5. (d) Phase-matching measurement results for $KNbSi_2O_7$, $PbZnSiO_4$, Na_2TiSiO_5 and KDP.

of recently reported silicate NLO materials, such as $Li_2K_4[(TiO)Si_4O_{12}]$ (4.5 × KDP) and $Li_2Rb_4[(TiO)Si_4O_{12}]$ (4.5 × KDP),[19] $Ba_2TiOSi_2O_7$ (5.5 × KDP),[17] $PbSrSiO_4$ (5.8 × KDP),[20] and $Sr_2ZnSi_2O_7$ (35 × α-SiO_2).[43] It is worth noting that Crosnier *et al.* has tested the SHG effect of $KNbSi_2O_7$ to get an estimate of the phase transition temperature and identify it as a good candidate for a nonlinear optical material.[35] Subsequently, Gopalakrishnan *et al.* measured the SHG intensity of $KNbSi_2O_7$ as 200 times that of α-SiO_2.[44] The above results support our calculations and experimental results. Afterwards, single crystals of $KNbSi_2O_7$ with a size of 10 × 10 × 1 mm^3 were fabricated.[45] In order to investigate the structure–property relationship, the NLO-related properties were calculated by using DFT method. The partial density of states (PDOS) (see Fig. 5(a)) reveals that the valence band maximum (VBM) is predominantly contributed by the orbitals of O nonbonding 2p. The main components of the conduction band minimum (CBM) are the 4d orbitals of Nb. The SHG-weighted densities presented in Fig. 5(b) and (c) illustrate that the electron densities that mainly contribute to SHG arise from O and Nb atoms in occupied and unoccupied states, respectively.

$PbZnSiO_4$ compound crystallizes in a NCS polar space group $Pna2_1$ and the cell parameters are a = 8.2441(1) Å, b = 18.96259(20) Å, c = 5.06(1) Å, $\alpha = \beta = \gamma = 90°$, Z = 8. In

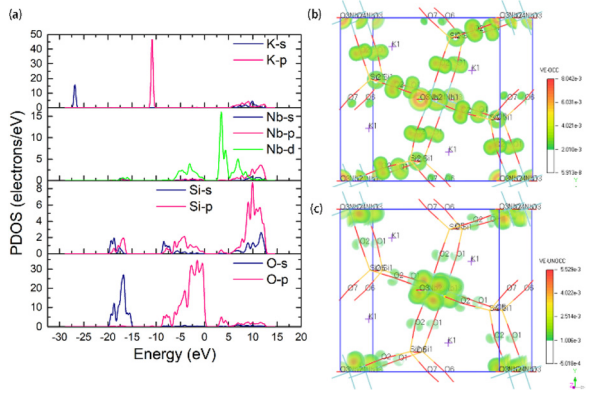

Fig. 5 (a) Partial DOS of $KNbSi_2O_7$, SHG density in the (b) occupied state and (c) unoccupied state of $KNbSi_2O_7$.

$PbZnSiO_4$, the 3D network is constructed by the ZnO_4 and the SiO_4 tetrahedron through shared corner O atoms. The Pb atoms are located in the vacancies of the network (see Fig. 3(b)). $PbZnSiO_4$ exhibits a UV cutoff edge of 276 nm and an absorption edge of 3.27 eV. The measured SHG response of $PbZnSiO_4$ is about 2.9 times that of KDP (Fig. 4(d)). The PDOS (see Fig. S4(a)†) reveals that the VBM is predominantly contributed by the nonbonding 2p orbitals of O. The main components of the CBM are predominantly contributed by the Pb 6p orbitals. One can easily find that the 6s orbitals of Pb appear at the VBM. This is the obvious character of the stereochemical active lone pair (SCALP) effect of the Pb atom. The SHG weighted density shows that the main source of electron density is the O atom in the occupied state (see Fig. S5(a)†) and Pb atoms and O atoms in the unoccupied state (see Fig. S5(b)†).

Na_2TiSiO_5 crystallizes in the crystal system and belongs to the $Pmc2_1$ space group with the cell parameters a = 9.1222(5) Å, b = 4.8040(3) Å, c = 9.8293(5) Å, $\alpha = \beta = \gamma = 90°$, Z = 4. The structural unit of Na_2TiSiO_5 is composed of two independent Na atoms, one Ti atom, two Si atoms and five O atoms. Each Si atom is coordinated by four O atoms to form a SiO_4 tetrahedron. Each Ti atom is coordinated by five O atoms to form a TiO_5 quadrangular pyramid. The compressed TiO_5 square pyramid connects with the SiO_4 group by sharing four bottom O atoms of TiO_5 to form a 3D network. The top O atoms are only coordinated with the Ti atom. The sodium ions are located in the voids of the structure to balance the charge of this anionic framework (see Fig. 3(c)). The short UV cutoff edge of Na_2TiSiO_5 is determined to be about 280 nm and its absorption edge is 3.66 eV. Na_2TiSiO_5 shows a SHG intensity 2.8 times that of KDP at 1064 nm laser irradiation (Fig. 4(d)). The PDOS (see Fig. S4(b)†) reveals that the VBM is predominantly contributed by the 2p orbitals of O. The main components of the CBM are predominantly contributed by the 3d orbitals of Ti. The SHG weighted density shown in Fig. S6 (a) and (b)† indicates that O atoms, especially the top O atoms in the TiO_5 quadrangular pyramid, are the main source in the occupied state. In the unoccupied state, the main sources are Ti atoms.

As shown in Table 1, one can find that cations have a significant effect on the band gap, birefringence, and SHG coeffi-

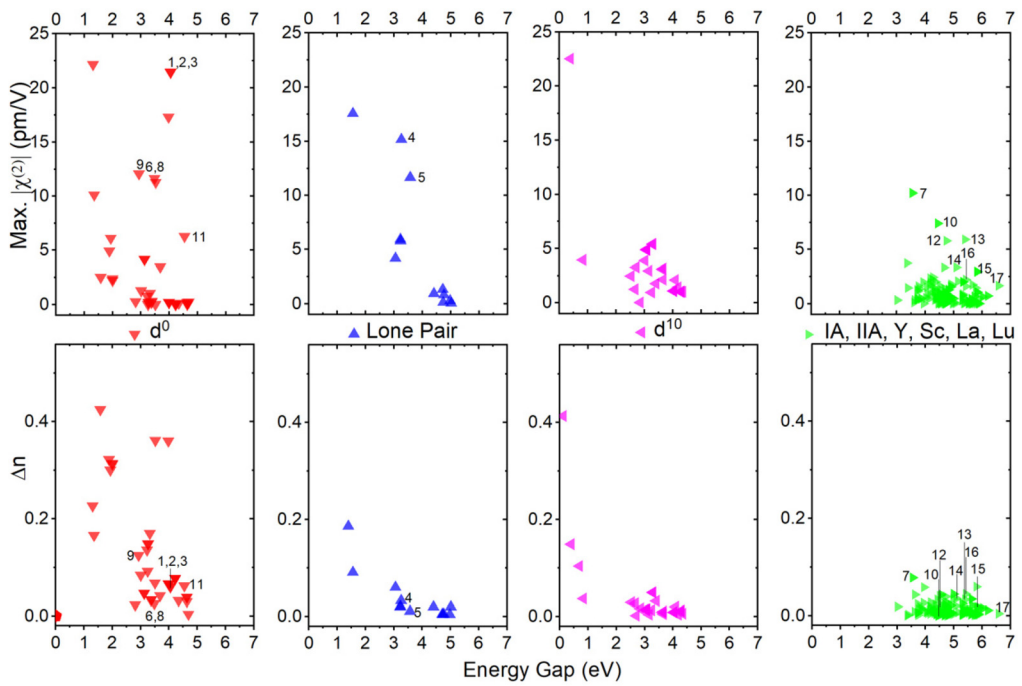

Fig. 6 Using GGA functionals the maximum $\chi^{(2)}$ and birefringence (Δn) *vs.* band gap calculated of 253 selected silicates divided into four categories: structures containing (1) d^0-TM cations, (2) lone pair (LP) cations, (3) d^{10}-TM cations, and (4) alkali metal and alkaline-earth metal cations.

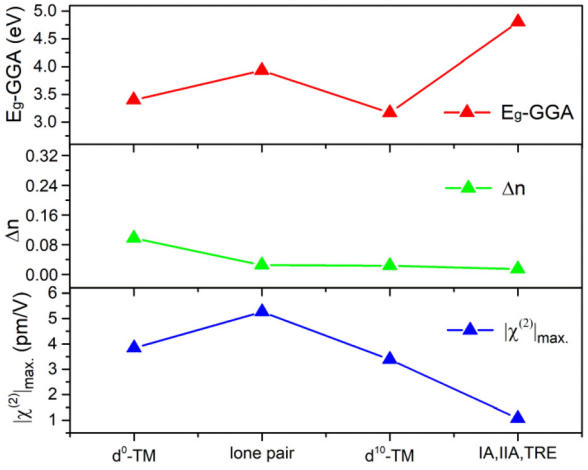

Fig. 7 Statistical average values of the band gap (E_g-GGA), maximum SHG tensor ($|\chi^{(2)}|_{max}$), and birefringence (Δn) of silicates that contain d^0-TM cations, LP cations, d^{10}-TM cations, alkalis, alkaline-earth metal cations, and trivalent rare-earth cations (IA, IIA, TRE).

cients. In order to clarify the influence of different cation types on NLO-related properties, the 253 structures are divided into four categories according to their cation types: (1) d^0-TM cations, (2) lone pair (LP) cations, (3) d^{10}-TM cations, and (4) alkalis and alkaline-earth metal cations as well as trivalent rare-earth (TRE) cations. If the crystal contains more than one kind of cation, the crystal will be classified as the former categories as listed above. As show in Fig. 6, the $\chi^{(2)}$ and Δn dispersions of different cations are obviously different. We count the average performance of 253 silicates according to the cation kinds. The duplicate structures are excluded from the statistic. As shown in Fig. 7, one can find that cation types have an obvious influence on the E_g, Δn, and $\chi^{(2)}$ values. The d^0-TM, LP, and d^{10}-TM cations reduce the band gap compared to the alkali/alkaline-earth/TRE metal cations. In contrast, they can induce larger $\chi^{(2)}$ and Δn. In particular, d^0-TM and LP cations can significantly improve the $\chi^{(2)}$ values.

Conclusion

In summary, an effective first-principles high-throughput screening pipeline (FHSP) based on the DFT method is adopted for the silicate system for searching for excellent NLO materials. Subsequently, 8 compounds are screened out by two-step calculation. Finally, $KNbSi_2O_7$, $PbZnSiO_4$, and Na_2TiSiO_5 are selected and synthesized successfully using the conventional solid-state method. $KNbSi_2O_7$ exhibits a large birefringence of 0.071 and a strong phase-matchable SHG intensity of 6.7 times that of KDP. $PbZnSiO_4$ and Na_2TiSiO_5 exhibit SHG intensities of 2.9 and 2.8 × KDP at 1064 nm, respectively. The UV absorption edges of the three title compounds are 243 nm, 276 nm, and 280 nm, respectively. Based on the statistic results of all the 253 silicates we calculated, one can find that the d^0-TM and LP cations are significant sources for SHG and birefringence and are the preferred choice for exploring new NLO materials in silicates. This work provides a full view of silicates to search for new NLO materials and obtain excellent candidates for the next step of development.

Conflicts of interest

The authors declare no competing financial interest.

Acknowledgements

This work was supported by the National Natural Science Foundation of China (grant No. 52072109, 21975062, and 22101069) and the Science and Technology Project of Hebei Education Department (grant No. BJK2023029 and QN2023234).

References

1 M. Mutailipu, K. R. Poeppelmeier and S. L. Pan, Borates: A rich source for optical materials, *Chem. Rev.*, 2021, **121**, 1130–1202.
2 J. Chen, C. L. Hu, F. F. Mao, J. H. Feng and J. G. Mao, A facile route to nonlinear optical materials: three-site aliovalent substitution involving one cation and two anions, *Angew. Chem., Int. Ed.*, 2019, **58**, 2098–2102.
3 C. F. Wu, J. W. Feng and F. Yu, Na: A new lanthanum sodium borate with infinite 2D layer 2 and moderate birefringence, *New J. Chem.*, 2021, **45**, 13592–13598.
4 W. Zhang, H. Yu, H. Wu and P. S. Halasyamani, Phase-matching in nonlinear optical compounds: A materials perspective, *Chem. Mater.*, 2017, **29**, 2655–2668.
5 L. Gao, J. Huang, S. Guo, Z. Yang and S. Pan, Structure–property survey and computer-assisted screening of mid-infrared nonlinear optical chalcohalides, *Coord. Chem. Rev.*, 2020, **421**, 213379.
6 F. Liang, L. Kang, Z. Lin, Y. Wu and C. Chen, Analysis and prediction of mid-IR nonlinear optical metal sulfides with diamond-like structures, *Coord. Chem. Rev.*, 2017, **333**, 57–70.
7 X. F. Lu, Z. H. Chen, X. R. Shi, Q. Jing and M. H. Lee, Two pyrophosphates with large birefringences and second-harmonic responses as ultraviolet nonlinear optical materials, *Angew. Chem., Int. Ed.*, 2020, **59**, 17648–17656.
8 L. Qi, Z. H. Chen, X. R. Shi, X. D. Zhang, Q. Jing, N. Li, Z. Q. Jiang, B. B. Zhang and M. H. Lee, $A_3BBi(P_2O_7)_2$ (A = Rb, Cs; B = Pb, Ba): Isovalent cation substitution to sustain large second-harmonic generation responses, *Chem. Mater.*, 2020, **32**, 8713–8723.
9 C. Chen, Y. Wang, Y. Xia, B. Wu, D. Tang, K. Wu, Z. Wenrong, L. Yu and L. Mei, New development of nonlinear optical crystals for the ultraviolet region with mole-

cular engineering approach, *J. Appl. Phys.*, 1995, **77**, 2268–2272.
10 C. Chen, Y. Wu, A. Jiang, B. Wu, G. You, R. Li and S. Lin, New nonlinear-optical crystal: LiB_3O_5, *J. Opt. Soc. Am. B*, 1989, **6**, 616–621.
11 R. L. Byer, M. M. Choy, R. L. Herbst, D. S. Chemla and R. S. Feigelson, Second harmonic generation and infrared mixing in $AgGaSe_2$, *Appl. Phys. Lett.*, 1974, **24**, 65–68.
12 S. C. Abrahams and J. L. Bernstein, Crystal structure of piezoelectric nonlinear-optic $AgGaS_2$, *J. Chem. Phys.*, 1973, **59**, 1625–1629.
13 G. D. Boyd, E. Buehler and F. G. Storz, Linear and nonlinear optical properties of $ZnGeP_2$ and CdSe, *Appl. Phys. Lett.*, 1971, **18**, 301–304.
14 M. C. Ohmer and R. Pandey, Emergence of chalcopyrites as nonlinear optical materials, *MRS Bull.*, 2013, **23**, 16–22.
15 V. M. Skorikov, I. S. Zakharov, V. V. Volkov and E. A. Spirin, Transmission and absorption spectra of $Bi_{12}GeO_{20}$, $Bi_{12}SiO_{20}$ and $Bi_{12}TiO_{20}$ single crystals, *Inorg. Mater.*, 2002, **38**, 172–178.
16 E. Burattini, G. Cappuccio, M. Grandolfo, S. M. Efendiev, P. Vecchia and M. C. Ferrari, Medium infrared transmittance and reflectance spectra of $Bi_{12}GeO_{20}$, $Bi_{12}SiO_{20}$, and $Bi_{12}TiO_{20}$ single crystals, *J. Opt. Soc. Am. B*, 1988, **5**, 714–720.
17 W. Zhao, F. Zhang, J. Liu, B. Hao, S. Pan, F. Zhang and L. Liu, Flux crystal growth of $Ba_2TiOSi_2O_7$, *J. Cryst. Growth*, 2015, **413**, 46–50.
18 M. J. Weber and P. D. Webber, *Handbook of optical materials*, CRC Press LLC, 2003.
19 T. L. Chao, W. J. Chang, S. H. Wen, Y. Q. Lin, B. C. Chang and K. H. Lii, Titanosilicates with strong phase-matched second harmonic generation responses, *J. Am. Chem. Soc.*, 2016, **138**, 9061–9064.
20 S. Jiang, J. Zhou, H. Wu, H. Yu, Z. Hu, J. Wang and Y. Wu, $PbSrSiO_4$: A new ultraviolet nonlinear optical material with a strong second harmonic generation response and moderate birefringence, *Chem. Commun.*, 2020, **56**, 7104–7107.
21 J. Yuan, P. Fu, J. Wang, F. Guo, Z. Yang and Y. Wu, A new nonlinear optical material $Sr_2TiSi_2O_8$, *Prog. Cryst. Growth Charact. Mater.*, 2000, **40**, 103–106.
22 H. Wu, H. Yu, S. Pan, Z. Huang, Z. Yang, X. Su and K. R. Poeppelmeier, $Cs_2B_4SiO_9$: A deep-ultraviolet nonlinear optical crystal, *Angew. Chem., Int. Ed.*, 2013, **52**, 3406–3410.
23 B. Zhang, X. Zhang, J. Yu, Y. Wang, K. Wu and M.-H. Lee, First-principles high-throughput screening pipeline for nonlinear optical materials: Application to borates, *Chem. Mater.*, 2020, **32**, 6772–6779.
24 S. K. Kurtz and T. T. Perry, A powder technique for the evaluation of nonlinear optical materials, *J. Appl. Phys.*, 1968, **39**, 3798–3813.
25 V. Milman, K. Refson, S. J. Clark, C. J. Pickard, J. R. Yates, S. P. Gao, P. J. Hasnip, M. I. J. Probert, A. Perlov and M. D. Segall, Electron and vibrational spectroscopies using DFT, plane waves and pseudopotentials: CASTEP implementation, *J. Mol. Struct.: THEOCHEM*, 2010, **954**, 22–35.
26 R. W. Godby, M. Schluter and L. J. Sham, Trends in self-energy operators and their corresponding exchange-correlation potentials, *Phys. Rev. B: Condens. Matter Mater. Phys.*, 1987, **36**, 6497–6500.
27 J. P. Perdew, K. Burke and M. Ernzerhof, Generalized gradient approximation made simple, *Phys. Rev. Lett.*, 1996, **77**, 3865–3868.
28 J. Heyd and G. E. Scuseria, Assessment and validation of a screened Coulomb hybrid density functional, *J. Chem. Phys.*, 2004, **120**, 7274–7280.
29 A. V. Krukau, O. A. Vydrov, A. F. Izmaylov and G. E. Scuseria, Influence of the exchange screening parameter on the performance of screened hybrid functionals, *J. Chem. Phys.*, 2006, **125**, 224106.
30 Z. Lin, X. Jiang, L. Kang, P. Gong, S. Luo and M.-H. Lee, First-principles materials applications and design of nonlinear optical crystals, *J. Phys. D: Appl. Phys.*, 2014, **47**, 253001.
31 J. Yu, B. Zhang, X. Zhang, Y. Wang, K. Wu and M. H. Lee, Finding optimal mid-infrared nonlinear optical materials in germanates by first-principles high-throughput screening and experimental verification, *ACS Appl. Mater. Interfaces*, 2020, **12**, 45023–45035.
32 F. G. Layman, Unit cell and space group of larsenite, $PbZnSiO_4$, *Am. Mineral.*, 1957, **42**, 910–912.
33 G. Bayer, O. W. Florke, W. Hoffman, *et al.*, Demixing and crystallization in glasses of the system Na_2O–TiO_2–SiO_2, *Glastech. Ber.*, 1966, **39**, 242–261.
34 W. Eysel and T. Hahn, Polymorphism and solid solution of Ca_2GeO_4 and Ca_2SiO_4, *Z. Kristallogr. – Cryst. Mater.*, 1970, **131**, 322–341.
35 M. P. Crosnier, D. Guyomard, A. Verbaere, Y. Piffard and M. Tournoux, $K_2(NbO)_2Si_4O_{12}$: A new material for nonlinear optics, *Ferroelectrics*, 1991, **124**, 61–66.
36 J. Gittins, E. L. Gasparrini and S. G. Fleet, The occurrence of vlasovite in Canada, *Can. Mineral.*, 1973, **12**, 211–214.
37 J. C. Shen and P. B. Moore, Crystal structure of cappelenite, $Ba(Y, RE)_6[Si_3B_6O_{24}]F_2$: A silicoborate sheet structure, *Am. Mineral.*, 1984, **69**, 190–195.
38 C. D. McMillen, M. Emirdag-Eanes, J. T. Stritzinger and J. W. Kolis, Hydrothermal synthesis of new rare earth silicate fluorides: A novel class of polar materials, *J. Solid State Chem.*, 2012, **195**, 155–160.
39 Z. Zhou, Y. Qiu, F. Liang, L. Palatinus, M. Poupon, T. Yang, R. Cong, Z. Lin and J. Sun, $CsSiB_3O_7$: A beryllium-free deep-ultraviolet nonlinear optical material discovered by the combination of electron diffraction and first-principles calculations, *Chem. Mater.*, 2018, **30**, 2203–2207.
40 W. Eysel and H. Theo, Polymorphism and solid solution of Ca_2GeO_4 and Ca_2SiO_4, *Z. Kristallogr.*, 1970, **131**, 322–341.
41 H. Kageyama, K. Hayashi, K. Maeda, J. P. Attfield, Z. Hiroi, J. M. Rondinelli and K. R. Poeppelmeier, Expanding frontiers in materials chemistry and physics with multiple anions, *Nat. Commun.*, 2018, **9**, 772.

42 R. A. Nyquist and R. O. Kagel, *Infrared spectra of inorganic compounds (3800–45 cm^{-1})*, Academic Press, New York, 1971.
43 M. Mutailipu, Z. Li, M. Zhang, D. Hou, Z. Yang, B. Zhang, H. Wu and S. Pan, The mechanism of large second harmonic generation enhancement activated by Zn^{2+} substitution, *Phys. Chem. Chem. Phys.*, 2016, **18**, 32931–32936.
44 J. Gopalakrishnan, K. Ramesha, K. Kasthuri Rangan and S. Pandey, In search of inorganic nonlinear optical materials for second harmonic generation, *J. Solid State Chem.*, 1999, **148**, 75–80.
45 A. Sahashi, T. Hoshina, H. Takeda and T. Tsurumi, Fabrication of ferroelectric silicate $KNbSi_2O_7$ single crystal, *J. Ceram. Soc. Jpn.*, 2014, **122**, 389–392.